# Correlation states of ethylene

S. J. Desjardins and A. D. O. Bawagan[a)]
*Ottawa-Carleton Chemistry Institute, Carleton University, Ottawa, Ontario K1S 5B6, Canada*

Z. F. Liu and K. H. Tan
*Canadian Synchrotron Radiation Facility, Synchrotron Radiation Center, University of Wisconsin, Stoughton, Wisconsin 53589*

Y. Wang and E. R. Davidson
*Department of Chemistry, Indiana University, Bloomington, Indiana 47405*

(Received 3 October 1994; accepted 19 January 1995)

High resolution synchrotron photoelectron spectra (PES) of ethylene have been obtained at several photon energies in the range 30 to 220 eV. Further evidence is presented that the correlation (satellite) peak at 27.4 eV binding energy is ''intrinsic'' in nature. A new correlation peak at 21.4 eV binding energy, however, is found to be a ''dynamic'' correlation. Several PES of 1-$^{13}$C-ethylene have also been obtained and have been found to be identical to those of normal ethylene. Both of the correlation peaks are also present in the labeled species with similar photon energy behaviors. Sophisticated theoretical calculations are found to agree quantitatively with the experimental PES spectra. © *1995 American Institute of Physics.*

## I. INTRODUCTION

The interpretation of photoelectron spectra has benefitted tremendously from molecular orbital models wherein the motion of electrons are considered to be independent of each other. These models are successful at predicting the main features of valence shell and inner shell photoelectron spectra, however they cannot account for the ''extra'' peaks that are often observed. These extra peaks in the experimental photoelectron spectra were initially called satellite or shake-up peaks, though the more proper name correlation peaks (For consistency, the experimental phenomena will be referred to as ''correlation peaks''[1] and the theoretical representation or interpretation of these phenomena as ''correlation states.''[2]) is preferable as it indicates the mechanism responsible for these features. It is precisely from the interactions (correlations) of electrons in atomic or molecular systems that these correlation peaks appear in the photoelectron spectra of many species.[3–28] The correlation states of atoms, especially the noble gas atoms, have been investigated intensely, however the study of these states in molecular systems is still in its infancy. This work presents perhaps one of the most thorough investigations of the correlations of a simple, nondiatomic molecule.

Schemes have been proposed, such as those by Becker and Shirley,[3] to classify correlation states and their production mechanisms by studying the photon energy dependence of the ratios of the satellite peak intensities to the main or ''parent'' peaks observed in the photoelectron spectra of noble gas atoms. The photon energy dependence of satellite/main peak intensities in photoelectron spectra has been investigated in pioneering studies by Wuilleumier and Krause.[4] The earlier x-ray studies were, however, hampered by poor energy resolution and many closely spaced satellites were not resolved. With the introduction of high intensity and high brilliance synchrotron sources, such photon energy dependence studies have now led to less ambiguous measurements of the satellite/main peak intensities. Those correlation (satellite) peaks that exhibit a constant ratio with increasing photon energy are referred to as intrinsic correlations and are considered to be caused by initial and/or final state configuration interaction;[1–3] whereas those correlation (satellite) peaks that exhibit a strong photon energy dependence in the satellite to main peak intensity ratio are referred to as dynamic correlations and can be produced by shake-up processes,[3–7] continuum state interactions,[3,7,9,10] or interchannel coupling.[3,6,7,29] The term ''shakeup'' is used here in a limited sense to refer only to correlation peaks that exhibit a particular photon energy dependence in their cross sections as discussed by Becker and Shirley.[3]

Several experimental and theoretical studies on atomic systems[3–22] have indicated that the phenomenological classification of correlation states into intrinsic and dynamic correlations is very useful in understanding the complexity of electron–electron interactions. Recent studies on molecular systems[23–28] have also shown that the Becker–Shirley classification is feasible. In particular, a recent study on a well-known correlation peak[27] of ethylene at 27.4 eV binding energy has revealed that this peak clearly results from intrinsic correlations. The satellite/main peak intensity ratio has been shown to be effectively constant over a wide photon energy range (40 to 1500 eV). Furthermore, comparisons of the experimentally derived satellite/main intensity ratio with theoretical multireference singles and doubles configuration interaction (MRSDCI) calculations by Murray and Davidson[30] indicated that quantitative agreement can be obtained. And so, highly sophisticated theoretical calculations can provide *quantitative* predictions of the photoelectron intensities of medium-sized molecules such as ethylene. This result is very encouraging for molecular investigations and illustrates the importance of high quality theoretical calculations and careful analysis of high resolution synchrotron photoelectron spectra.

Ethylene $[C_2H_4(D_2h)]$ has the following electronic

a)To whom correspondence should be addressed.

configuration in the ground state: $(1a_g)^2(1b_{1u})^2(2a_g)^2(2b_{1u})^2(1b_{2u})^2(3a_g)^2(1b_{3g})^2(1b_{3u})^2$, having $^1A_g$ symmetry. All orbital symmetries are referenced to the molecule lying in the $yz$ plane, with the C–C double bond along the $z$ axis.

The photoelectron spectrum (PES) of ethylene, the simplest unsaturated hydrocarbon, has been investigated extensively both experimentally[12,27,28,31–34] and theoretically.[30,34–41] The PES of the carbon $2s$ region of ethylene was first reported by Gelius[12] using Al $K\alpha$ x rays (1487 eV) in 1974. It was also reported by Berndtsson *et al.*[31] in 1975 and subsequently studied by Banna and Shirley[32] with Mg $K\alpha$ (1253 eV) and Y $M_\zeta$ (132 eV) x-ray sources. According to self-consistent field (SCF) calculations, the peaks at 23.7 and 19.2 eV binding energy were assigned as $2a_g$ and $2b_{1u}$ primary ionization peaks, respectively. The strong satellite at 27.4 eV, with an intensity of 39% of the $2a_g$ primary peak in the Mg $K\alpha$ spectrum[32] was originally assigned as a $^2B_{1u}$ (considering the molecule to be in its proper $yz$ orientation) correlation state.[12,31,32] The task of the earlier theoretical calculations[41–51] was to assign the five main bands (below 20 eV binding energy) through Koopmans' Theorem at the Hartree–Fock (HF) level. The first study that went beyond the HF approximation (Green's function method[35]) was published in 1976. Martin and Davidson[36] performed a small configuration interaction (CI) calculation on the ethylene cation which agreed with experimental PES results, but indicated that the intense satellite at 27.4 eV belonged to the $^2A_g$ symmetry manifold, with a calculated intensity of 30% of the primary $2a_g$ peak. Subsequent electron momentum spectroscopy (EMS) experiments,[42,43] also known as binary $(e,2e)$ spectroscopy, confirmed this symmetry assignment; however, the satellite/main peak intensity ratios obtained were different. Differences in the correlation peak intensity ratios between EMS and PES have previously been observed in argon $3s^{-1}$ ionization spectra.[21] Investigation into the nature of these differences are actively being pursued.[44–47]

Cederbaum *et al.*[37] performed Green's function calculations, including more correlation configurations in their investigation than Martin and Davidson,[36] but used smaller basis sets without diffuse Rydberg functions. The results agreed qualitatively with experiment, but the calculations predicted a much richer structure than can be experimentally resolved. Two $^2A_g$ correlation states of roughly equal intensity less than 1 eV apart centered at 23.5 eV and another two closely spaced $^2A_g$ correlation states centered at 27.5 eV were found. The intensity of this dual satellite (27.5 eV) was found to be 24% of the dual primary peak (23.5 eV).[37] The recent MRSDCI calculation of Murray and Davidson[30] with the Cederbaum basis set[37] lead to a conclusion similar to the previous work of Martin and Davidson,[36] as neither calculation produced the twinning phenomenon of the $^2A_g$ peak at 23.5 eV binding energy.

In addition to these earlier calculations, Baker[38] investigated the PES of ethylene using the EOM/propagator technique. Two $^2A_g$ correlation states of roughly the same intensity centered at 23.2 eV were found, but only one $^2A_g$ correlation state at 27.26 eV. Truncation of the virtual space caused the twinning phenomenon to disappear for the case of the satellite state. Two calculations based on the symmetry-adapted cluster (SAC) expansion CI theory performed by Nakatsuji[39] and Wasada and Hirao[40] are also of interest as no twinning of the $^2A_g$ primary peak was observed, nor was there any strong $^2A_g$ satellite between 27.0 and 30.0 eV binding energy. Furthermore, the 27.4 eV satellite peak was assigned back to $^2B_{1u}$ symmetry contrary to most of the other theoretical calculations.[36,37]

TABLE I. Summary of theoretical calculations.

| Reference | Method[a] | Calculated intensity ratio[b] | Comment[a] |
|---|---|---|---|
| Martin and Davidson (Ref. 36) | MRSDCI | 30% | no twinning |
| Cederbaum *et al.* (Ref. 37) | MBPT | 24% | twinning |
| Murray and Davidson (Ref. 30) | MRSDCI | 35% | no twinning |
| Baker (Ref. 38) | EOM | 23% | partial twinning |
| Present work | CI $1p$-$2h$ | 35% | no twinning |
| | MRSDCI (MO) | 35% | twinning |
| | MRSDCI (ANO) | 35% | twinning |

[a]See the text for details.
[b]Satellite (27.4 eV) to main peak intensity ratio.

In all of these previous calculations, the overall size of the basis set was never larger than 70-CGTO. The present work is aimed at resolving the discrepancies among the different approaches, through the use of a larger basis set (196-CGTO). A concise summary of the theoretical approaches and predicted intensity ratios for the 27.4 eV correlation state is shown in Table I.

In the present study, the well-known correlation peak at 27.4 eV binding energy, assigned to the $^2A_g$ symmetry manifold,[36] has been confirmed as an intrinsic correlation[27] based on additional experimental data. Also, more evidence of the dynamic nature of the newly discovered[28] correlation peak at 21.4 eV has been obtained based on PES spectra of normal ethylene and $^{13}C$ labeled ethylene. The interesting photon energy dependence of the new correlation state is extensively discussed.

## II. EXPERIMENTAL DETAILS

The synchrotron photoelectron spectra (PES) were obtained at the Canadian Synchrotron Radiation Facility (CSRF) at the Aladdin Storage Ring of the University of Wisconsin at Madison's Synchrotron Radiation Center (SRC). The spectra were collected using the McPherson photoelectron spectrometer equipped with a multichannel plate detector[48] in conjunction with both the grasshopper grazing incidence monochromator[49] with high and low energy gratings and the 3 m toroidal grating monochromator (3 m-TGM),[50] also with high and low energy gratings. Angular corrections are not required as the photoelectrons were collected at the pseudomagic angle.[51] All reported intensity ratios were corrected for analyzer transmission effects.[25] Further background corrections were made for low energy scattered electrons and stray light for the data obtained with the 3 m-TGM which provided most of the lower photon

energy PES spectra. A single Matheson Gas Products research purity (99.99%) sample of ethylene was used for all experimentation. Further experiments were also conducted with isotopically labeled ethylene (1-$^{13}$C-ethylene) from Isotec (99% pure). Note that this particular sample has one $^{13}$C atom whereas the other carbon atom is ''normal'' $^{12}$C.

The transmission of the spectrometer has been thoroughly investigated using neon $2s$ and $2p$ ionization cross sections for calibration studies. The transmission of the spectrometer is found to be linear in electron kinetic energy above 20 eV; below this energy, the transmission is relatively constant.[25] Gaussian curves are fitted to the Ne peaks according to known experimental energy resolutions, using the program Peakfit (version 3). The areas (intensities) of the Gaussian fitted peaks were obtained and the appropriate intensity ratios derived. Intensity ratios of photoelectron peaks are corrected for transmission effects; these corrections range from approximately 20% at 45 eV down to approximately 2% at 200 eV. The intensity of second order radiations from the CSRF grasshopper monochromator was also investigated via the $2p$ peak of neon and it was found that second order radiation is of significant intensity only at photon energies lower than those over which the spectra were obtained. The second order radiation maximizes in intensity (approximately 40%) between 30 and 35 eV primary photon energy, but quickly falls off, down to approximately 1% of the first order intensity by 45 eV. The total experimental energy resolution, including both electron analyzer and monochromator effects, was found to range from 490 meV FWHM at 45 eV to 820 meV FWHM at 200 eV. For the spectra obtained with the 3 m-TGM, the low energy scattering of electrons caused an exponential-decay-like low kinetic energy background which made a further correction necessary. ''No gas'' background spectra were run in conjunction with the ethylene spectra at the various photon energies; these background spectra were then scaled (all points multiplied by a constant) to match the low kinetic energy tail of the ethylene spectra. The background spectra were then subtracted from the ethylene spectra and the resulting spectra were then analyzed with the same procedure as the other (grasshopper) spectra. The error limits shown in the transmission corrected intensity ratios refer to statistical uncertainties arising from curve fitting alone. Systematic errors due to the assumed base line and transmission function are estimated to be less than 10%.

## III. THEORETICAL BACKGROUND

The Hartree–Fock (HF) approximation for the ground state wave function of a neutral molecule can be represented as $\Psi_{\mathrm{HF}}(N)$, where $N$ represents the number of electrons in the system. Ionization can then be represented by the primary hole configuration wave function $\Phi_k(N-1)$, which corresponds to removal of an electron from the $k$th occupied orbital. If $a_k$ is an annihilation operator that destroys orbital $k$ in $\Psi_{\mathrm{HF}}(N)$, then

$$\Phi_k(N-1)=a_k\Psi_{\mathrm{HF}}(N). \tag{1}$$

If there are $n$ occupied orbitals in $\Psi_{\mathrm{HF}}(N)$, then the spectrum should consist of $n$ primary peaks. Koopmans' Theorem states that, to the extent these approximations are accurate, these peaks will be at positions given by the negative of the orbital energies.

However, the appearance of correlation peaks in photoelectron spectra proves the inadequacy of simple single-particle methods. Ionic configurations can also be formed by a combination of excitations and ionizations. The one-particle two-hole ($1p$-$2h$) configuration involves the removal of two electrons from the ground state configuration; one is lost by ionization, the other is excited to a virtual orbital of the ground state. This configuration can be represented as

$$\Phi^r_{kl}(N-1)=a_k a_l a^{\dagger}_r\Psi(N), \tag{2}$$

where $k$ and $l$ are the occupied orbitals involved in the excitation and ionization processes and $a^{\dagger}_r$ is a creation operator that places an electron in virtual orbital $r$. If these configurations were true states of the ion, then the ion should have excitation energies corresponding to the differences between them and the ground state of the ion. Since photoionization is dominated by one-electron dipole mechanisms, the intensities of the peaks associated with these states would be zero.

All configurations, $0p$-$1h$ (primary hole), $1p$-$2h$, $2p$-$3h$ (two-particle, three-holes), etc. are required to form a complete set of functions. Therefore the wave function for any state of the ion is written as a linear combination of all possible configurations:

$$\Psi_{\mathrm{ion}}=\sum_{k=1}^{n} C_k\Phi_k(N-1)+\sum_{klr} C^r_{kl}\Phi^r_{kl}(N-1)+\cdots, \tag{3}$$

where the $C$'s are configuration interaction (CI) coefficients and the first sum is over the $n$ $0p$-$1h$ configurations of the ion corresponding to the primary peaks. In simplified notation the $j$th eigenstate of the cation can be written as

$$\Psi_j(N-1)=\sum_p C_{pj}\Phi^{(p)}(N-1), \tag{4}$$

where $C_{pj}$ is a coefficient that describes the extent of configuration mixing and $\Phi^{(p)}(N-1)$ is the $p$th possible ion configuration ($0p$-$1h$, $1p$-$2h$, etc.). Similarly the ground state of the neutral molecule can be represented as

$$\Psi(N)=\sum_q D_q\Phi^{(q)}(N), \tag{5}$$

where $\Phi^{(q)}(N)$ describes the $q$th possible configuration of the neutral molecule (i.e., HF, $1p$-$1h$, $2p$-$2h$, etc.) and $D_q$ is the CI coefficient for the $q$th configuration.

The pole strength (probability) for the $j$th ionic state is defined by the square of the norm:

$$S^2_j=\|\langle\Psi_j(N-1)|\Psi(N)\rangle_{N-1}\|^2=\left\|\sum_{p,q} C^*_{pj}D_q s_{pq}\right\|^2, \tag{6}$$

where

$$s_{pq}=\langle\Phi^{(p)}(N-1)|\Phi^{(q)}(N)\rangle_{N-1} \tag{7}$$

and the subscript on the bracket indicates integration over only $N-1$ electrons.

Further the Dyson orbital can be defined as

$$\varphi^j_{\text{Dyson}} = S_j^{-1}\langle \Psi_j(N-1)|\Psi(N)\rangle_{N-1} = S_j^{-1}\sum_{p,q} C^*_{pj} D_q s_{pq} \tag{8}$$

which allows the transition moment (the square of which is proportional to the intensity)

$$M_j = \langle \Psi_j(N-1)\chi^j(k)|\mu|\Psi(N)\rangle \tag{9}$$

to be written as

$$M_j = \langle \chi^j(k)|\mu|\varphi^j_{\text{Dyson}}\rangle S_j\,, \tag{10}$$

where $\chi^j(k)$ is the continuum function for the outgoing (ejected) electron associated with state $j$ and $\mu$ is the dipole operator.

If initial state configuration interaction (ISCI) and final ionic state configuration interaction (FISCI) are considered, correlation peaks generally arise through transitions to high energy states of the *same symmetry* as the associated primary hole state. The intensity ratio of the $j$th satellite (correlation) peak to the $p$th primary peak is given by[1,2]

$$\frac{I(j,k')}{I(p,k)} \approx \frac{M_j^2}{M_p^2} = \frac{|S_j\langle \chi^j(k')|\mu|\varphi^j_{\text{Dyson}}\rangle|^2}{|S_p\langle \chi^p(k)|\mu|\varphi^p_{\text{Dyson}}\rangle|^2}. \tag{11}$$

For most satellites (correlation states) it is possible to identify a primary hole state ($0p$-$1h$) such that $\varphi^j_{\text{Dyson}} \approx \varphi^p_{\text{Dyson}}$. In this case,

$$\frac{I(j)}{I(p)} \approx \frac{S_j^2}{S_p^2} \tag{12}$$

if the comparison is made at the same outgoing photoelectron kinetic energy (i.e., $k' \approx k$) and if $\chi^j$ is sufficiently similar to $\chi^p$ in the region of space close to the molecule. If the satellite/main intensity ratio is computed at the same photon energy then it must further be assumed that the dipole transition matrix elements do not change rapidly with $k$. For the present study this condition holds favorably since the kinetic energies are $>10$ eV. Furthermore, the coupling of channels in the continuum is neglected.[1,2] With these approximations, Eq. (12) is formally equivalent to the sudden approximation of Åberg[52] in the limit $k \to \infty$. In the present approximation the explicit form of the continuum function is not specified. It is only assumed that the continuum functions are similar for the states being compared (i.e., for the relative ratios).

For a qualitative understanding of the PES spectrum a single determinant HF wave function is assumed for the initial neutral state. For the $p$th primary hole state, the coefficient of one $0p$-$1h$ configuration is assumed to be dominant. In a correlation state, all of the $0p$-$1h$ coefficients are small, but one of the $0p$-$1h$ coefficients is assumed to be much larger than the others. In this case, the intensity ratio of the $j$th satellite peak to the $p$th primary peak involving the same $0p$-$1h$ dominant configuration is[1,2,36]

$$\frac{I(j)}{I(p)} \approx \frac{C_{pj}^2}{C_{pp}^2}. \tag{13}$$

TABLE II. Calculated ionization energies together with the experimental binding energies of the primary and intense satellite peaks in the PES of ethylene.

| Orbital | SCF ionization energy (eV) | MRSDCI (ANO) ionization energy (eV) | Experimental binding energy (eV) |
|---|---|---|---|
| $1b_{3u}$ | 10.2 | 10.38 | 10.5[a] |
| $1b_{3g}$ | 13.8 | 12.91 | 12.9[a] |
| $3a_g$ | 15.9 | 14.66 | 14.7[a] |
| $1b_{2u}$ | 17.5 | 16.02 | 15.9[a] |
| $2b_{1u}$ | 21.5 | 19.24 | 19.2[b] |
| $2a_g$ | 28.1 | 23.3, 24.5 | 23.7[b] |
| | | 27.7, 28.7 | 27.4[b] |

[a]From Ref. 31.
[b]From Ref. 32.

It has been observed that with FISCI and without ISCI, the intensities were satisfactory in the aggregate but very wrong in detail;[53] however, with both FISCI and ISCI, the agreement of the theoretical PES spectrum with experiment was much better.

A 196-CGTO basis set, defined later, was used in three different sets of configuration interaction calculations. Both final and initial state CI was included. The calculated energies of the PES peaks have been shifted slightly from the calculated values shown in Table II so that the primary peak from each symmetry agrees with its experimental position.[30] The results of the calculations are shown in Table III and Figs. 12 and 13.

## IV. RESULTS AND DISCUSSION

### A. The intrinsic correlation state

Figures 1 and 2 show sample synchrotron photoelectron spectra of normal ethylene, taken at 91.1 and 59.5 eV photon energy, respectively, having peaks associated with ionization from the six valence molecular orbitals. The energy scale was calibrated by aligning the binding energy of the $1b_{3u}$ peak (10.51 eV) with high resolution He I spectra.[54] The extra peak, labeled ''sat,'' is the well-known correlation peak originally observed by Gelius.[12] Note that further improvements in the experimental energy resolution up to $\sim$150 meV FWHM does not better resolve the inner valence region. The present widths of the inner valence peaks correspond closely to their natural linewidths which is consistent with the fact that these are largely dissociative states.

Figure 3 shows a sample spectrum of $^{13}$C-labeled ethylene (1-$^{13}$C–$C_2H_4$) at 59.5 eV photon energy. It can be seen that the PES spectrum of isotopically labeled ethylene (Fig. 3) is very similar to that of normal ethylene (Fig. 2) at the same photon energy with regards to binding energies, peak areas, and peak widths, further confirming that the extra structure (labeled sat) found in the PES is of ''electronic origins,'' i.e., largely independent of nuclear structure. It is well-known that vibrational frequencies, and thus the Franck–Condon widths associated with photoionization, are influenced by deuterium substitution of the hydrogen atoms in ethylene.[55] In this particular experiment, $^{13}$C substitution will also change the vibrational frequencies of ethylene and thus decrease the Franck–Condon widths associated with

TABLE III. The calculated line positions and intensities for the PES of ethylene[a] [the MRSDCI (ANO) calculation].

| Symmetry | Root index | Ionization energy[b] (eV) | Intensity[c] $S_j^2$ | Important configurations[d] |
|---|---|---|---|---|
| $A_g$ | 1 | 14.7 | 0.81 | $0.93(3a_g)^{-1}$ |
| | | | | $0.16(3a_g)^{-1}(1b_{3u})^{-2}(1b_{2g})^{2}$ |
| | 2 | 22.1 | 0.00 | $0.95(1b_{3u})^{-2}(na_g)^{1}$ |
| | 3 | 23.4 | 0.19 | $0.77(1b_{3u})^{-2}(na_g)^{1}$ |
| | | | | $0.46(2a_g)^{-1}$ |
| | | | | $0.28(2b_{1u})^{-1}(1b_{3u})^{-1}(1b_{2g})^{1}$ |
| | 4 | 24.6 | 0.28 | $0.59(1b_{3u})^{-2}(na_g)^{1}$ |
| | | | | $0.55(2a_g)^{-1}$ |
| | | | | $0.45(2b_{1u})^{-1}(1b_{3u})^{-1}(1b_{2g})^{1}$ |
| | 5 | 25.1 | 0.02 | $0.92(1b_{3u})^{-2}(na_g)^{1}$ |
| | | | | $0.19(2b_{1u})^{-1}(1b_{3u})^{-1}(1b_{2g})^{1}$ |
| | | | | $0.15(2a_g)^{-1}$ |
| | 7 | 27.1 | 0.02 | $0.71(2b_{1u})^{-1}(1b_{3u})^{-1}(1b_{2g})^{1}$ |
| | | | | $0.40(3a_g)^{-1}(1b_{3u})^{-2}(1b_{2g})^{2}$ |
| | | | | $0.34(1b_{3u})^{-2}(na_g)^{1}$ |
| | | | | $0.16(2a_g)^{-1}$ |
| | 8 | 27.6 | 0.01 | $0.92(1b_{3u})^{-2}(na_g)^{1}$ |
| | | | | $0.14(2b_{1u})^{-1}(1b_{3u})^{-1}(1b_{2g})^{1}$ |
| | | | | $0.11(2a_g)^{-1}$ |
| | 9 | 27.8 | 0.03 | $0.84(3a_g)^{-1}(1b_{3u})^{-1}(nb_{3u})^{1}$ |
| | | | | $0.27(3a_g)^{-1}(1b_{3u})^{-2}(1b_{2g})^{2}$ |
| | | | | $0.20(2b_{1u})^{-1}(1b_{3u})^{-1}(1b_{2g})^{1}$ |
| | | | | $0.18(2a_g)^{-1}$ |
| | 10 | 28.61 | 0.09 | $0.49(2b_{1u})^{-1}(1b_{3u})^{-1}(1b_{2g})^{1}$ |
| | | | | $0.43(1b_{3g})^{-2}(na_g)^{1}$ |
| | | | | $0.37(3a_g)^{-1}(1b_{3u})^{-2}(1b_{2g})^{2}$ |
| | | | | $0.29(2a_g)^{-1}$ |
| | 11 | 28.64 | 0.01 | $0.79(3a_g)^{-1}(1b_{3u})^{-1}(nb_{3u})^{1}$ |
| | | | | $0.47(1b_{3u})^{-2}(na_g)^{1}$ |
| | | | | $0.10(3a_g)^{-1}(1b_{3u})^{-2}(1b_{2g})^{2}$ |
| | | | | $0.09(2a_g)^{-1}$ |
| | | | | $0.03(3a_g)^{-1}$ |
| | 12 | 28.9 | 0.04 | $0.71(1b_{3g})^{-2}(na_g)^{1}$ |
| | | | | $0.27(3a_g)^{-1}(1b_{3u})^{-2}(1b_{2g})^{2}$ |
| | | | | $0.25(2b_{1u})^{-1}(1b_{3u})^{-1}(1b_{2g})^{1}$ |
| | | | | $0.24(1b_{2u})^{-2}(na_g)^{1}$ |
| | | | | $0.20(2a_g)^{-1}$ |
| | 13 | 29.1 | 0.02 | $0.76(1b_{3u})^{-2}(na_g)^{1}$ |
| | | | | $0.35(3a_g)^{-1}(1b_{3u})^{-1}(nb_{3u})^{1}$ |
| | | | | $0.19(2b_{1u})^{-1}(1b_{3u})^{-1}(1b_{2g})^{1}$ |
| | | | | $0.16(2a_g)^{-1}$ |
| | 15 | 29.9 | 0.01 | $0.78(1b_{2u})^{-1}(1b_{3u})^{-1}(1b_{1g})^{1}$ |
| | | | | $0.37(1b_{3g})^{-1}(1b_{3u})^{-2}(1b_{1g})^{1}(1b_{2g})^{1}$ |
| | | | | $0.26(1b_{3u})^{-2}(na_g)^{1}$ |
| | | | | $0.10(2a_g)^{-1}$ |
| $B_{3u}$ | 1 | 10.5 | 0.81 | $0.95(1b_{3u})^{-1}$ |
| | 2 | 23.9 | 0.00 | $0.92(1b_{3u})^{-2}(2b_{3u})^{1}$ |
| | | | | $0.11(1b_{3u})^{-1}(1b_{2u})^{-1}(2b_{2u})^{1}$ |
| $B_{2u}$ | 1 | 15.9 | 0.71 | $0.88(1b_{2u})^{-1}$ |
| | | | | $0.33(1b_{3g})^{-1}(1b_{3u})^{-1}(1b_{2g})^{1}$ |
| | | | | $0.11(1b_{2u})^{-1}(1b_{3u})^{-2}(1b_{2g})^{2}$ |
| | 2 | 18.2 | 0.02 | $0.93(1b_{3g})^{-1}(1b_{3u})^{-1}(1b_{2g})^{1}$ |
| | | | | $0.14(1b_{2u})^{-1}$ |
| | 3 | 22.1 | 0.06 | $0.80(1b_{3g})^{-1}(1b_{3u})^{-1}(1b_{2g})^{1}$ |
| | | | | $0.28(1b_{2u})^{-1}(1b_{3u})^{-2}(1b_{2g})^{2}$ |
| | | | | $0.22(1b_{2u})^{-1}$ |
| $B_{1u}$ | 1 | 19.2 | 0.61 | $0.82(2b_{1u})^{-1}$ |
| | | | | $0.41(3a_g)^{-1}(1b_{3u})^{-1}(1b_{2g})^{1}$ |
| | | | | $0.13(2a_g)^{-1}(1b_{3u})^{-1}(1b_{2g})^{1}$ |
| | 2 | 20.3 | 0.06 | $0.91(3a_g)^{-1}(1b_{3u})^{-1}(1b_{2g})^{1}$ |
| | | | | $0.26(2b_{1u})^{-1}$ |
| | 3 | 23.4 | 0.0050 | $0.94(1b_{3u})^{-2}(nb_{1u})^{1}$ |

TABLE III. (*Continued.*)

| Symmetry | Root index | Ionization energy[b] (eV) | Intensity[c] $S_j^2$ | Important configurations[d] |
|---|---|---|---|---|
| | | | | $0.07(2b_{1u})^{-1}$ |
| | 4 | 24.3 | 0.08 | $0.83(3a_g)^{-1}(1b_{3u})^{-1}(1b_{2g})^1$ |
| | | | | $0.26(2b_{1u})^{-1}$ |
| | | | | $0.23(2b_{1u})^{-1}(1b_{3u})^{-2}(1b_{2g})^2$ |
| $B_{3g}$ | 1 | 12.9 | 0.79 | $0.92(1b_{3g})^{-1}$ |
| | | | | $0.16(1b_{2u})^{-1}(1b_{3u})^{-1}(1b_{2g})^1$ |
| | | | | $0.14(1b_{3g})^{-1}(1b_{3u})^{-2}(1b_{2g})^2$ |
| | 2 | 21.9 | 0.00 | $0.94(1b_{2u})^{-1}(1b_{3u})^{-1}(1b_{2g})^1$ |
| | 3 | 24.2 | 0.01 | $0.70(1b_{2u})^{-1}(1b_{3u})^{-1}(1b_{2g})^1$ |
| | | | | $0.57(1b_{3g})^{-1}(1b_{3u})^{-2}(1b_{2g})^2$ |
| $B_{2g}$ | 1 | 17.2[e] | 0.02 | $0.94(1b_{3u})^{-2}(nb_{2g})^1$ |
| | | | | $0.11(3a_g)^{-1}(1b_{3u})^{-1}(nb_{1u})^1$ |
| $B_{1g}$ | 1 | 34.6[f] | | |
| $A_u$ | 1 | 43.7[f] | | |

[a]For each symmetry, the MRSDCI wave functions were used for the cation and the neutral molecule and all calculations were based on the average natural orbitals except for the $B_{1g}$ and $A_u$ symmetries (see the text for details).

[b]The first root energies have been adjusted to experimental data separately for each symmetry. The same constant shift was used for the rest of the roots in that symmetry.

[c]The values less than 0.005 were ignored.

[d]The absolute values for the CI coefficients were taken.

[e]The energy of the ground state of the neutral molecule was taken as the average value (−78.408 693 42 hartree) from the other 5-root calculation results. The second root of this symmetry lies at 25.9 eV with an intensity less than 0.005.

[f]The energy of the ground state of the neutral molecule was taken as the average value (−78.408 693 42 hartree) from the other 5-root calculation results. The energy of this symmetry was from the $1p$-$2h$ CI calculation result. The pole strength is less than $10^{-4}$.

outer valence ionization. High resolution PES with supersonic molecular beams have been able to resolve the outer valence vibrational structure of ethylene;[56] however, the present study is more concerned with the inner valence and satellite regions. For the inner valence region $^{13}C$ substitution is a reasonably sensitive test of ''nuclear effects'' in correlation states. $^{13}C$ substitution introduces an asymmetric 1/12 change in nuclear mass of one of the carbons. If these extra peaks are not purely electronic effects but are influenced by some electron–nuclear scattering process, then there should be some differences in their inner valence PES. No detectable difference is observed (cf. Figs. 2 and 3), thus ''nuclear effects'' as a possible factor contributing to the satellite structure in the photoelectron spectrum of ethylene is discounted. The present results lend further support to current theoretical approaches to the interpretation of correlation peaks as arising from solutions of the *electronic* many-body Schrödinger equation for both the neutral and final ionic states. Although non-Born–Oppenheimer (nonadiabatic) effects have been predicted and observed in the outer valence photoelectron spectrum of ethylene, they are seen to be relatively small effects.[57,58] Another theoretical study on vibronic coupling effects in the inner valence photoelectron spectrum of acetylene[59] showed no significant intensity borrowing between different satellite states. The present study on normal ethylene and $^{13}C$-labeled ethylene is part of a growing number of explorations of nonadiabatic effects in the inner valence region of PES spectra and seems to support the earlier theoretical studies.[57,59]

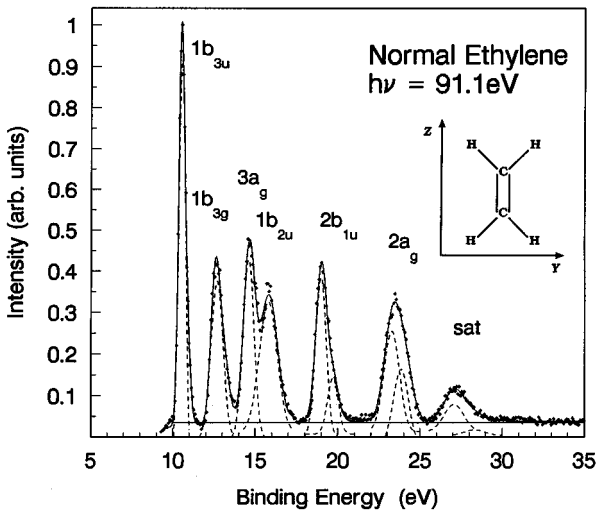


FIG. 1. Synchrotron PES spectrum of normal ethylene at 91.1 eV. The curve-fitting model used for all of the spectra is shown by the dashed Gaussians and the solid base line. Single Gaussian peaks are fitted to the experimental peaks attributed to ionization from the outer valence orbitals. Two Gaussian peaks of equal widths are fitted to each of the experimental peaks attributed to the satellite (27.4 eV), $2a_g^{-1}$ and $1b_{1u}^{-1}$. The sum of the peaks is represented as a solid line. The spectrum as shown is not corrected for transmission effects. The estimated total experimental energy resolution is 470 meV FWHM. The standard orbital notation assumes $D_{2h}$ symmetry with the molecule in the $yz$ plane (see inset diagram).

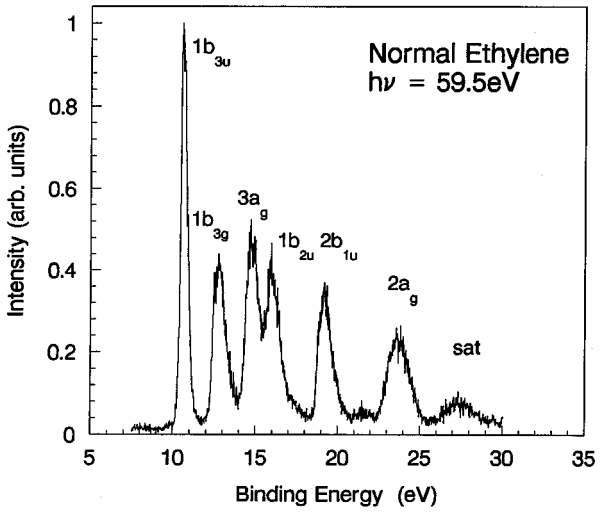


FIG. 2. PES of normal ethylene taken at 59.5 eV. The spectrum as shown is not corrected for transmission effects.

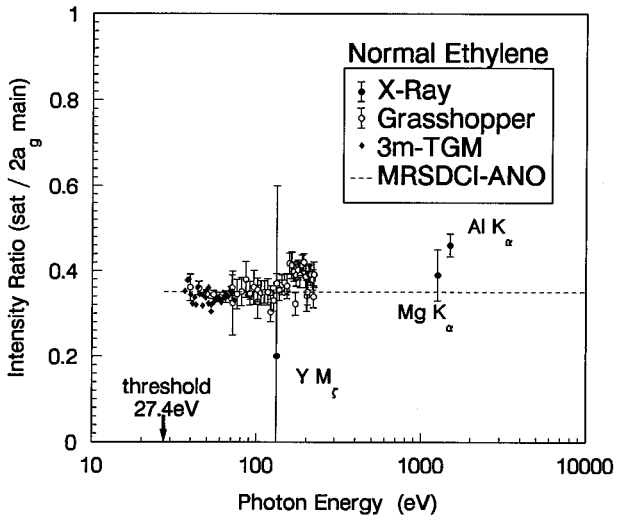


FIG. 4. Photon energy dependence of the 27.4 eV major satellite/main $2a_g^{-1}$ peak intensity ratios derived from synchrotron PES measurements for normal ethylene. The experimentally derived ratios are corrected for transmission effects. The open circles with error bars are data from the grasshopper monochromator and the solid diamonds are data from the 3 m-TGM. Previous x-ray measurements (Refs. 31 and 32) are shown as solid circles. The dashed line is the predicted satellite/main intensity ratio from the MRSDCI(ANO) calculation (see Table III).

The correlation peak at 27.4 eV has been thoroughly investigated by measuring the satellite/main $2a_g^{-1}$ peak intensity ratio at different photon energies from 40 to 220 eV. These ratios are presented in Fig. 4, with previous x-ray measurements also shown for comparison. The approximately constant trend reported previously[27] is seen to continue at the lower photon energies, approaching the threshold. Very close to threshold ($h\nu<40$ eV), the condition $k' \approx k$ does not hold and Eq. (12) is not rigorously valid thus slight variations are expected. PES at photon energies less than $h\nu=36$ eV are difficult to obtain with the present electrostatic photoelectron energy analyzer. The difficulty arises from background problems associated with low energy scattered electrons. The dashed line represents the ratio (0.35) calculated from the MRSDCI(ANO) calculation (see Sec. IV C). The high value for Al $K\alpha$ is probably a result of experimental factors unaccounted for as the published spectrum was deconvoluted using a peak profile similar to that used for the fitting of the synchrotron spectra. Figure 5 shows the photon energy dependence of the correlation peak at 27.4 eV in the case of 1-$^{13}$C-ethylene. The dashed line also represents the same MRSDCI(ANO) calculation shown in Fig. 4. The constant value of the intensity ratio observed in both normal (Fig. 4) and labeled (Fig. 5) ethylene is indicative of an intrinsic correlation, using the notation of Becker and Shirley,[3] a result of initial and/or final state configuration interaction. These configuration interactions are always occuring, and the photoionization process only allows them to be seen—it does not produce them—thus, there should be no photon energy dependence expected within the conditions discussed in Sec.

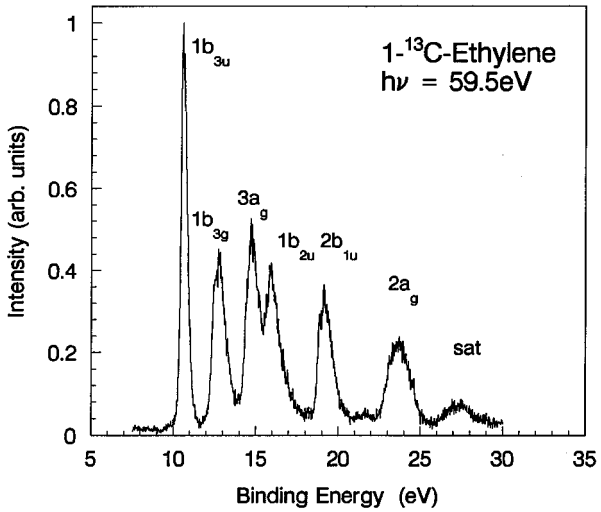


FIG. 3. PES of 1-$^{13}$C-ethylene taken at 59.5 eV. The spectrum as shown is not corrected for transmission effects. The isotopically labeled ethylene is seen to have a similar spectrum to that of normal ethylene.

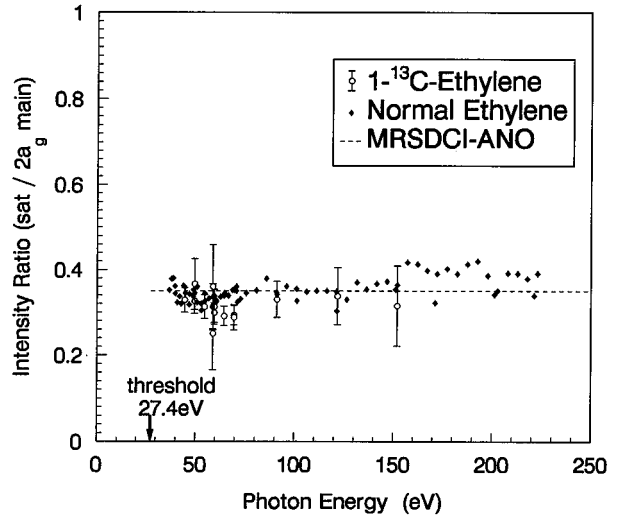


FIG. 5. Photon energy dependence of the 27.4 eV major satellite/main $2a_g^{-1}$ peak intensity ratios for 1-$^{13}$C-ethylene. The ratios are corrected for transmission effects and shown as open circles with error bars. The ratios for normal ethylene are shown as solid diamonds for comparison.

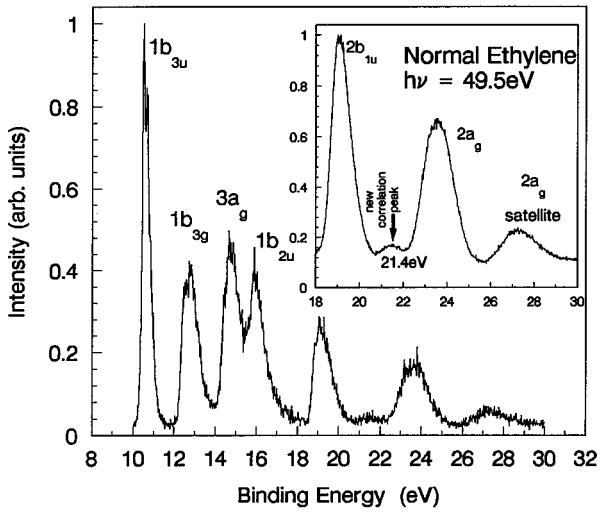


FIG. 6. Main: A representative photoelectron spectrum of normal ethylene taken at 49.5 eV photon energy with a total energy resolution of 360 meV FWHM. Insert: A section of the photoelectron spectrum of ethylene obtained with several scans highlighting the new correlation peak at 21.4 eV binding energy between the $2b_{1u}$ and $2a_g$ peaks. The peak at 27.4 eV binding energy is produced by intrinsic correlations (Ref. 27). The spectra as shown are not corrected for transmission effects.

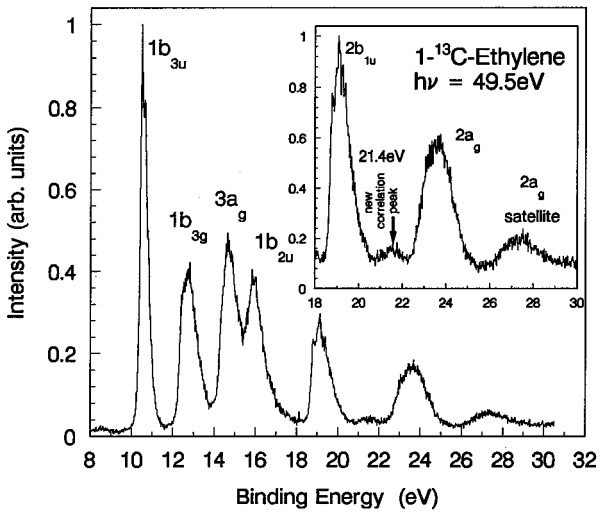


FIG. 7. Main: A representative photoelectron spectrum of 1-$^{13}$C-ethylene taken at 49.5 eV to show that the PES is similar to that of normal ethylene, having the same new correlation peak at 21.4 eV with the same intensity. Insert: Another spectrum obtained with better statistics to highlight the new correlation peak. The spectra as shown are not corrected for transmission effects.

III. The threshold has been approached, within the limitations of the current instrumentation, yet the constant trend has been observed to continue, providing further evidence against contributions from mechanisms like shake-up or interchannel coupling. The excellent quantitative agreement between experiment and theory (as shown by the dashed line in Figs. 4 and 5) indicates that the theoretical understanding of the $^2A_g$ correlation peak at 27.4 eV is on a solid foundation. The calculations are discussed in detail in Sec. IV C.

### B. The dynamic correlation state

A new correlation peak at 21.4 eV binding energy is observed in the synchrotron photoelectron spectrum of ethylene taken at 49.5 eV photon energy (see Fig. 6). The same correlation peak can be observed in a previously reported He II spectrum,[33] however it was not acknowledged in that particular study. Because of the low intensity of this peak, it is quite easy to consider the peak as part of the background. Only a variable photon energy experiment can unambiguously identify a low-intensity peak of this nature. A 1978 Green's function calculation by Cederbaum *et al.*[37] did predict an intrinsic correlation state between the $2b_{1u}$ and $2a_g$ main peaks, associated with the $2b_{1u}$ peak. The new correlation peak at 21.4 eV has a well-defined peak shape (1.5 eV FWHM) and is found to have significant intensity over a certain photon energy range. The same satellite peak is also observed in the synchrotron PES of $^{13}$C-labeled ethylene in the same range of photon energies (see Fig. 7). An investigation of the pressure dependence of the photoionization cross section has shown that the correlation peak at 21.4 eV is not a result of inelastic processes. The intensity ratio of the new correlation peak to the $2b_{1u}$ main peak was found to vary by less than 4% over an order of magnitude of change in pressure. Nor is the new satellite caused by Auger processes or second order radiations. The peak binding energy position was found to be constant with changing photon energy and the experiments were conducted at photon energies where second order radiation is inconsequential. Furthermore, there is a consistent agreement between the two sets of experimental data obtained on two different synchrotron beamlines (i.e., CSRF grasshopper and SRC 3 m-TGM). In addition, the only previous report of this correlation peak using He II radiation shows reasonable agreement with the synchrotron results, indicating that the results obtained in the present study are not caused by any experimental artifact.

The ratio of the new correlation peak intensity to the intensity of the $2b_{1u}$ peak for normal ethylene as a function of photon energy is shown in Fig. 8. The $2b_{1u}$ main peak is tentatively chosen as the primary peak associated with the new correlation peak for convenience. The present results are independent of this choice since the photon energy dependences of the $2a_g/2b_{1u}$ and $1b_{2u}/2b_{1u}$ intensity ratios are *constant* in the photon energy range of the current investigation. The experimentally derived new correlation peak/$2b_{1u}$ intensity ratio clearly shows a strong photon energy dependence and would appear to be a result of dynamic correlations. The new peak has significant intensity only at lower photon energies, i.e., less than 70 eV, and is virtually unnoticeable beyond 150 eV, thus explaining why this peak was not observed in previous high resolution x-ray photoelectron spectra.[31,32,34] Bieri and Åsbrink[33] detected this peak in their He II work, but did not make any comment as to its origin. Their published experimental spectrum has been digitized and deconvoluted like the synchrotron PES to obtain a value for the satellite to $2b_{1u}$ main peak ratio which is also shown in Fig. 8. The large error bar associated with this point is indicative of the uncertainty resulting from the digitization of the published spectrum and the lack of knowledge of the background and transmission characteristics of the spectrometer used. Also, the He II work was conducted at $\theta=90°$, thus

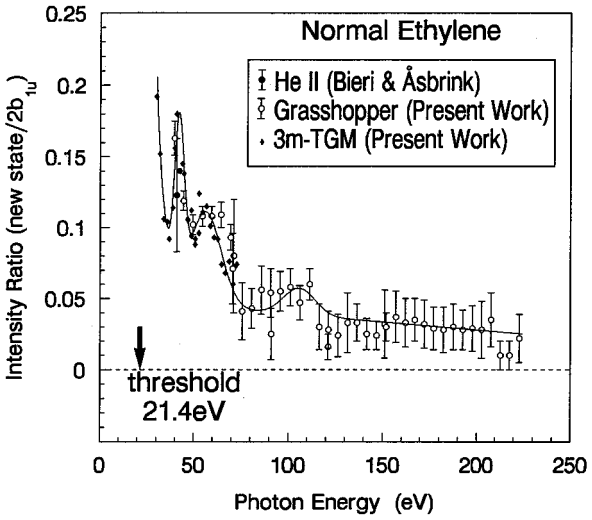


FIG. 8. Ratio of the intensity of the new correlation peak to the intensity of the $2b_{1u}^{-1}$ peak as a function of photon energy for normal ethylene. All reported ratios are corrected for transmission effects. The He II result (solid circle with error bar) was calculated from a spectrum originally published in Ref. 33 and was not corrected for $\beta$ factor and transmission effects. The open circles with error bars are results from the grasshopper monochromator, the solid diamonds from the 3 m-TGM, and the solid line serves to highlight the resonance-like features at 42, 57, and 105 eV photon energy.

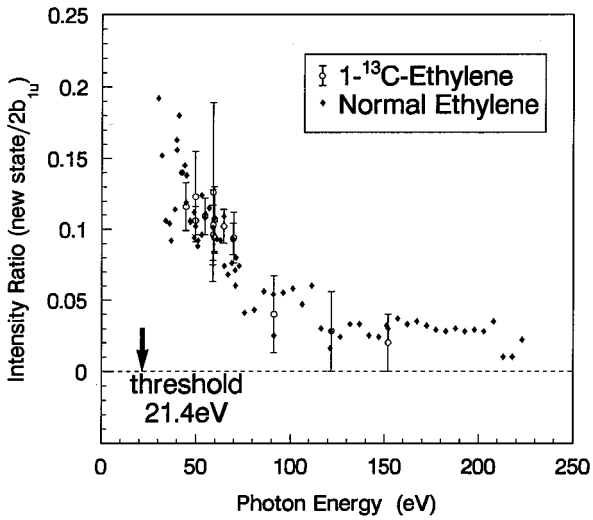


FIG. 9. Intensity ratio of the new correlation peak to the $2b_{1u}^{-1}$ main peak as a function of photon energy for 1-$^{13}$C-ethylene. The ratio values have been corrected for transmission effects. The data are shown as open circles with error bars; the ratio values for normal ethylene are shown as solid diamonds.

requiring an angular correction to the ratio. This slight correction is not known and was not applied to the data (see Fig. 8).

The photoionization differential cross sections for unpolarized He II radiation are of the form

$$\frac{d\sigma}{d\Omega}=(\sigma_0/4\pi)[1-(\beta/4)(3\ \cos^2\ \theta-1)], \tag{14}$$

where $\beta$ is the angular asymmetry parameter and $\theta$ is the relative angle between the outgoing photoelectron and the photon propagation direction. Since $\theta=90°$,

$$\frac{d\sigma}{d\Omega}=(\sigma_0/4\pi)[1+(\beta/4)] \tag{15}$$

and so the intensity ratio for the He II work is then of the form

$$\left[\frac{I(\mathrm{sat})}{I(2b_{1u})}\right]_{\mathrm{He\ II}}=\frac{\sigma_0(\mathrm{sat})\{1+[\beta(\mathrm{sat})/4]\}}{\sigma_0(2b_{1u})\{1+[\beta(2b_{1u})/4]\}}. \tag{16}$$

The synchrotron work is conducted at the pseudomagic angle, and so requires no angular correction. The intensity ratio here is

$$\left[\frac{I(\mathrm{sat})}{I(2b_{1u})}\right]_{\mathrm{synchrotron}}=\frac{\sigma_0(\mathrm{sat})}{\sigma_0(2b_{1u})}. \tag{17}$$

The double ratio (i.e., the ratio of the two intensity ratio values) is given by

$$\frac{[I(\mathrm{sat})/I(2b_{1u})]_{\mathrm{He\ II}}}{[I(\mathrm{sat})/I(2b_{1u})]_{\mathrm{synchrotron}}}=\frac{\{1+[\beta(\mathrm{sat})/4]\}}{\{1+[\beta(2b_{1u})/4]\}}. \tag{18}$$

Since the double ratio is approximately 1 (within the experimental and calculation uncertainty), as can be seen in Fig. 8, there is some evidence that $\beta(\mathrm{sat})\approx\beta(2b_{1u})$, supporting the suggestion that the $2b_{1u}$ peak could be the primary peak associated with the 21.4 eV correlation peak.

The ratio of the new correlation peak to $2b_{1u}$ for labeled ethylene is shown in Fig. 9 for comparison. Although there are fewer data points, the $^{13}$C-labeled ethylene data are clearly consistent with the general trend obtained for normal ethylene (Fig. 8).

There are two interesting points to note regarding the photon energy dependence of the intensity of this new correlation peak of ethylene at 21.4 eV (see Fig. 8):

(i) the general trend is increasing satellite/$2b_{1u}$ intensity ratio reaching $\approx$20% as the threshold (21.4 eV) is approached;

(ii) superimposed on this general trend are three ''resonance-type'' features located at photon energies of 42, 57, and 105 eV.

The features of the photon energy dependence curve are unexpected. The resonance-type features or the oscillations in the photon energy dependence curve can be characterized further as shown in Fig. 10. The new-peak/$2b_{1u}$ intensity ratio photon energy dependence can be approximated reasonably well with an exponential decay. Following the Becker–Shirley scheme, the intensity can be interpreted as being composed of three components: an intrinsic correlation component (the constant value, 0.021, which is similar to the behavior of the major satellite at 27.4 eV binding energy), a dynamic component [the exponential decay, like continuum state configuration interaction (CSCI)], and an oscillating component. The intrinsic and dynamic components are shown in Fig. 10 and the oscillating component in Fig. 11. The constant (intrinsic) and the exponential (dynamic) were fitted to the data. The data can be seen to exhibit oscillatory behavior around the exponential decay. The intensity ratio values are defined as

$$\text{Intensity ratio}=a[e^{-\epsilon/b}+\lambda(\epsilon)+c], \tag{19}$$

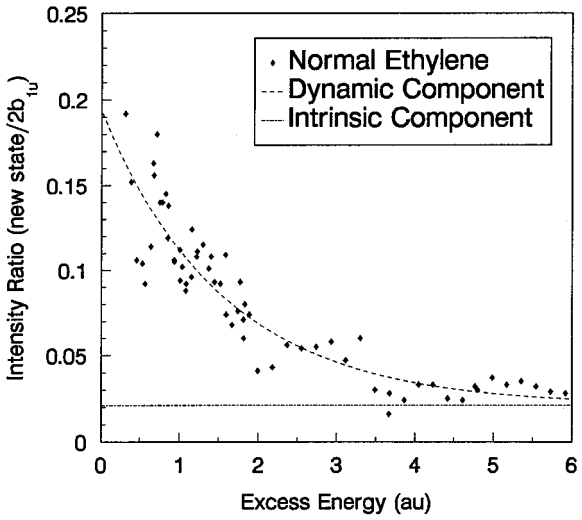


FIG. 10. The decomposition of Fig. 8. The intensity ratio values of the new correlation peak/$2b_{1u}^{-1}$ for normal ethylene are shown as solid diamonds. The photon energy dependence has been decomposed into three components: intrinsic, dynamic, and oscillating (see the text for details). The intrinsic component (constant) is shown as a dot–dash line; the dynamic component (exponential decay) is shown as a dashed line; and the oscillating component is shown in Fig. 11(a). The data are plotted vs scaled excess energy. The threshold energy of 21.4 eV has been subtracted from the photon energies, with the results being converted to atomic units by dividing the differences by 27.21 eV.

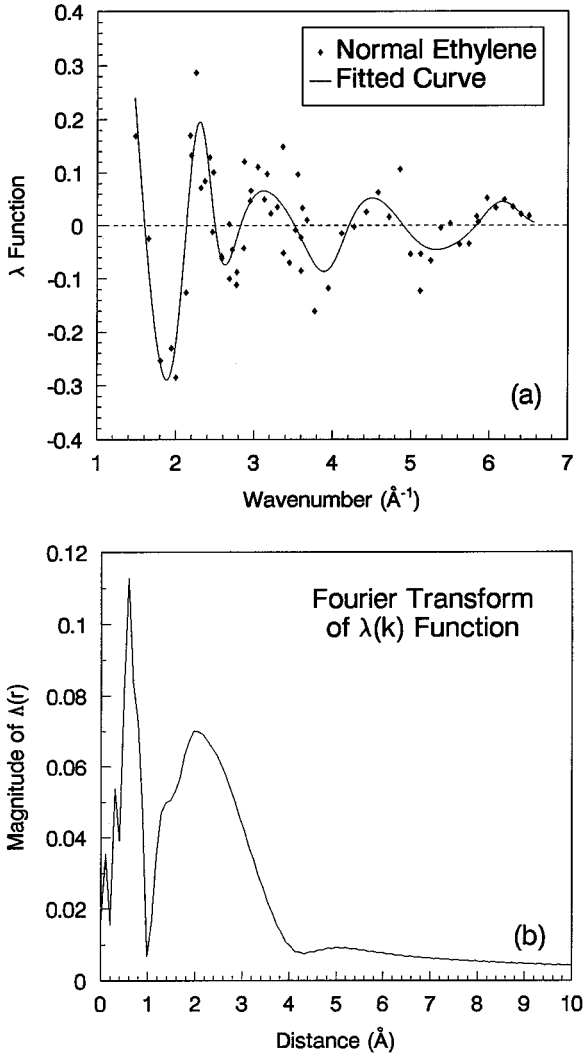


FIG. 11. (a) The oscillating part of the decomposition of Fig. 8. The $\lambda(k)$ function (plotted in $Å^{-1}$) is obtained by subtracting the constant and the exponential decay from the intensity ratio values and then converting to wave numbers. The solid diamonds are the experimental values and the solid line is a fitted curve, generated from fitting parameters. (b) The $\Lambda(r)$ function is the fast Fourier transform (FFT) of $\lambda(k)$. Two major characteristic distances are seen for the oscillating component, with values of $(0.6\pm0.1)$ and $(2.2\pm0.2)$ Å.

where $a$, $b$, and $c$ are constants (obtained from fitting to the intensity ratio data) and $\epsilon$ is the scaled excess energy (the threshold energy of 21.4 eV is subtracted from the photon energies, the resulting values are then converted to atomic units). The components can then be seen to be: intrinsic$=ac$; dynamic$=ae^{-\epsilon/b}$; and oscillating$=a\lambda(\epsilon)$. The intrinsic and dynamic components were subtracted from the data. The resulting pure oscillating component was then converted from scaled excess energy to wave numbers, and the function $\lambda(k)$ is plotted in Fig. 11(a). The parameters from the curve fitting were then used to generate a smooth curve for $\lambda(k)$ [see Fig. 11(a)] with equally spaced intervals of $k$ through a simple FORTRAN program. The oscillating component curve was then Fourier transformed using a fast Fourier transform (FFT) routine to extract characteristic distances from the oscillations. The FFT of the $\lambda(k)$ function $\Lambda(r)$ is shown in Fig. 11(b). The major characteristic distances are then $(0.6\pm0.1)$ and $(2.2\pm0.2)$ Å, which are of molecular dimensions. Note that the C–C bond length in ethylene is 1.34 Å.

### C. Theoretical calculations

In an attempt to gain an understanding of the origin and symmetry of the new correlation state at 21.4 eV, we carried out a series of theoretical calculations of the photoelectron spectrum of ethylene. A 196-CGTO basis set is used in the calculations. The $(18s13p)$ Partridge basis set[60] was chosen as the primitive basis for carbon. For hydrogen, Partridge's $(10s)$ basis[61] was used. For C, the first 14 $s$ functions were contracted into 2 $s$ functions using the $1s$ and $2s$ atomic orbital coefficients. Similarly, the first seven $p$ functions were contracted into one $p$ function using the $2p$ atomic orbital coefficients. For H, the first six $s$ functions were contracted into one $s$ function using the $1s$ atomic orbital coefficients. The rest of the functions were left uncontracted. This scheme lost less than 0.1 kcal/mol in a trial SCF calculation[62] on $CH_4$. All of the polarization functions were taken from Dunning.[63] For carbon, $(3d1f)$ ($\alpha_d=1.848$, 0.649, 0.228; $\alpha_f=0.761$) polarization functions were used; for hydrogen, $(2p1d)$ ($\alpha_p=1.257$, 0.355; $\alpha_d=0.916$) were used. This basis was further augmented by putting two $p$ and two $d$ diffuse Rydberg functions on the center of the C–C bond with exponents of 0.052 and 0.104 for both $p$ and $d$ functions. All Cartesian components were kept for $d$ and $f$ functions. Therefore, the final basis set was $[6s7p3d1f/5s2p1d]++++$, or 196-CGTO for short. To keep the results directly comparable, the same geometry as before[30,36] was used.

The first level of approximation to the spectrum was from the SCF calculation. The MO energies of the ground

state are compared with experimental peak positions in Table II. It is easy to see that the MO picture is not adequate to describe the location of the primary peaks and is, of course, unable to explain the appearance of the satellites. With this large basis set, the MO energies are nearly identical to the previous calculations[30,35,39,40] showing that the SCF orbital energies have converged.

The second level of approximation was to include all $1p$-$2h$ configurations in the final ionic state CI calculation with the full virtual space hereafter called the CI $1p$-$2h$ calculation. The lowest 15 roots of the CI matrix for each symmetry were calculated. The CI $1p$-$2h$ results are shown in Fig. 12(a), where only pole strengths greater than 0.005 are included. No ground state CI calculation was done. The square of the CI coefficient of the leading $0p$-$1h$ configuration in $\Psi(N-1)$ was used as the pole strength and the energies are taken relative to the experimental positions of the first primary peak of each symmetry. A strong $^2A_g$ satellite line at 28.8 eV is observed which has only 17% of the intensity of the primary $^2A_g$ peak. This calculation did not show the twinning phenomenon of either the primary or satellite $^2A_g$ peak. The computational details of the CI $1p$-$2h$ calculation are available.[64]

The third level of approximation was to perform a MRSDCI calculation for the lowest 15 roots of the CI matrix of each symmetry using molecular orbitals of the neutral ground state (i.e., $K$ orbitals[64]) hereafter called the MRSDCI(MO) calculation. The MRSDCI(MO) results are shown in Fig. 12(b). Pole strengths less than 0.005 are ignored. The square of the coefficients of the leading $0p$-$1h$ configuration in $\Psi(N-1)$ was used as the pole strengths. When the CI $1p$-$2h$ calculation is compared with the MRSDCI(MO) calculation, it is seen that after the improvement of the final ion state wave function, not only the intensities, but also the line positions change. Some twinning structure also appears as a result of the configuration interaction. The former $^2A_g$ primary peak at 23.7 eV moves to 23.9 eV, while the formerly weak satellite at 24.7 eV moves to 23.6 eV, but with twice the intensity, causing twinning centered at about 23.7 eV where the first line at 23.6 eV is not as strong as the one at 23.9 eV. The former 26.3 eV satellite shifts to 25.3 eV with nearly four times more intensity. The former 28.8 eV satellite splits into two pairs of dual lines (27.78, 27.80 eV) and (28.8, 29.6 eV). In the first pair, the peak at 27.78 eV is much stronger, whereas in the second pair, the intensity of the first peak is only slightly larger. For most peaks, $0p$-$1h$ and $1p$-$2h$ configurations are the leading configurations, while $2p$-$3h$ configurations are less important. The computational details of the MRSDCI(MO) calculation are available.[64]

It should be noted that the line position cannot be predicted by simply writing down the main configurations and summing the energies of each individual process. For example, the correlation state at 27.78 eV has the following leading configuration: $(2b_{1u})^{-1}(1b_{3u})^{-1}(1b_{2g})^{1}$, which in the common notation is

$$0.37(2b_{1u})^{-1}\ {}^3(\pi,\pi^*)-0.52(2b_{1u})^{-1}\ {}^1(\pi,\pi^*), \tag{20}$$

a $1p$-$2h$ configuration. For the transition $(\pi,\pi^*)$, there are

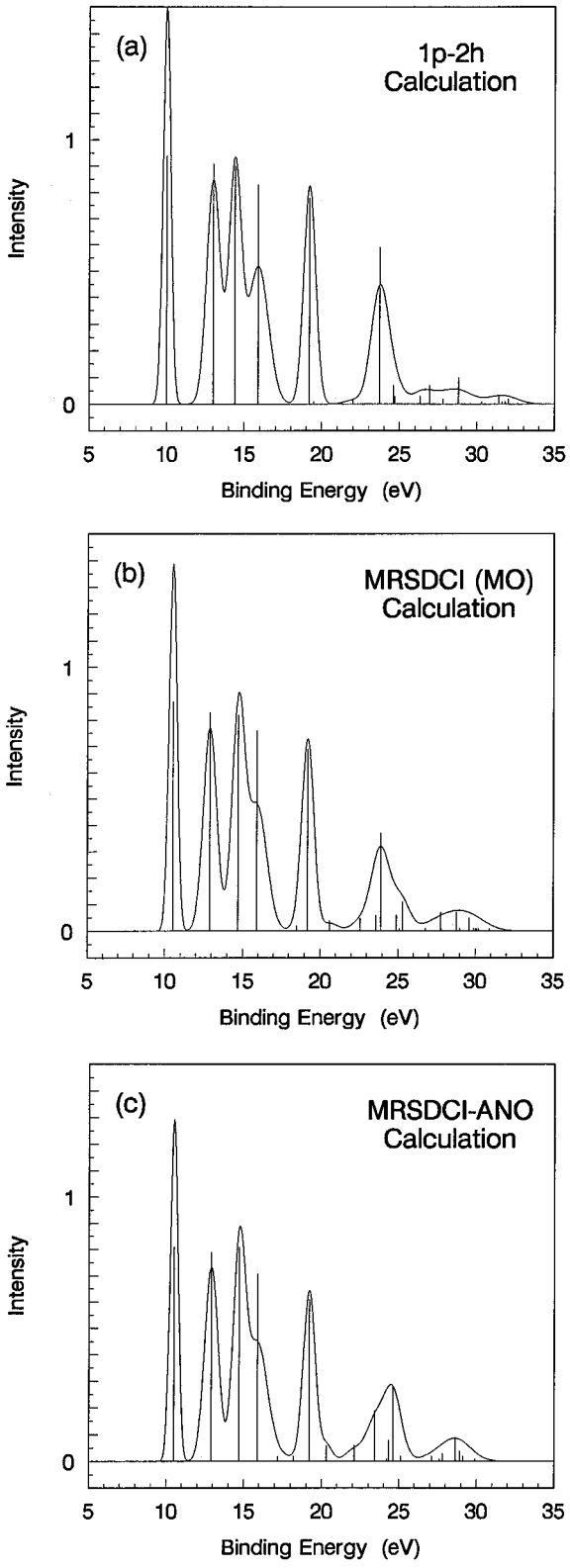


FIG. 12. The theoretical PES calculated using the theoretical line positions with the experimental peak widths. (a) The theoretical PES drawn using the intensity data from the CI $1p$-$2h$ calculation. (b) The theoretical PES drawn using the intensity data from the MRSDCI(MO) calculation. (c) The theoretical PES drawn using the intensity data from Table III [the MRSDCI(ANO) calculation].

two different excitation energies: 4.6 eV for the $T$ state,[65] $^3(\pi,\pi^*)$ and 7.65 eV for the $V$ state,[55] $^1(\pi,\pi^*)$. The ionization potential for the $2b_{1u}$ orbital is 19.2 eV. After summing the energies of the individual processes, the results are 26.85 eV for $(2b_{1u})^{-1}\,{}^1(\pi,\pi^*)$ and 23.8 eV for $(2b_{1u})^{-1}\,{}^3(\pi,\pi^*)$. Neither of the two values matches 27.78 eV or the experimental value 27.4 eV. Based on the above simple calculations, Gelius[12] discarded the $^2A_g$ assignment to the satellite line at 27.4 eV. The above method always gives lower energy than experimental values. Lindholm and Åsbrink[41] produced a detailed discussion about this problem, but through a semiempirical method, HAM/3.

To ease the comparison of the calculations with the experimental PES, the experimental linewidth for each line was used in conjunction with the calculated intensities to produce theoretical PES. Comparing the CI $1p$-$2h$ calculation [Fig. 12(a)] and the MRSDCI (MO) calculation [Fig. 12(b)], it is easily seen that the MRSDCI (MO) calculation improved the predicted PES spectrum for the satellite region, but produced a worse shape for the $^2A_g$ primary peak at 23.7 eV.

Because of the poor agreement of the above calculations with experiment, ion and neutral MRSDCI calculations based on the average natural orbitals (ANOs) were then performed. The ANOs based on states of a given symmetry were obtained from the average density matrix for the first 15 roots from the former ion MRSDCI calculation on that symmetry. For each symmetry, the lowest 15 roots for the cation were calculated and a MRSDCI calculation for the ground state of the neutral molecule using the same ANOs was performed and, to approximate the intensities, the pole strengths were obtained. The final MRSDCI (ANO) results are shown in Table III and the corresponding theoretical PES can be found in Fig. 12(c). More detailed information of all these MRSDCI (ANO) calculations are available.[64] Table II shows the actual primary peak positions as calculated. In Table III and Fig. 12(c) these have been shifted slightly so that the first peak of each symmetry agrees with experiment.

A MRSDCI calculation (using the ANOs for both the neutral molecule and the cation) on the $^2B_{2g}$ symmetry manifold was done, although there is no primary peak corresponding to this symmetry. In the neutral ground state, the configuration $\pi^{*2}\leftarrow\pi^2$ has the second largest weight and may give observable intensity through the overlap with the ion configuration $\pi^{-2}\pi^*$, which belongs to the $^2B_{2g}$ symmetry. The final MRSDCI calculation shows that only the first root of this symmetry has observable intensity ($S_j^2\approx 0.02$) and it lies at 17.2 eV.

When the MRSDCI(ANO) calculation is compared to the MRSDCI(MO) calculation, it can easily be seen that the states of $^2A_g$ symmetry have been improved for both the primary peak and the satellite region. From Table III and Fig. 12(c), it can also be seen that with this calculation, the satellite has nearly the same shape as the experimental results,[27,28] with about 35% of the intensity of the $^2A_g$ primary peak, although the line separation is overestimated by $\sim$0.3 eV. After comparing the important configurations for each peak, it should be noted that in Fig. 12(c), the peak at 23.4 eV, which corresponds to the 23.6 eV line in Fig. 12(b), gets more intensity, whereas the peak at 23.9 eV in Fig. 12(b) moves to 24.6 eV in Fig. 12(c), while losing some intensity, making the ''twinning phenomenon'' more obvious. The peak at 25.1 eV [25.3 eV in Fig. (12b)] becomes very weak. The $^2B_{2g}$ satellite at 17.2 eV acts as the long tail of the $^2B_{2u}$ primary peak at 15.9 eV. There are four candidates for the new correlation peak at 21.4 eV binding energy. A $^2B_{1u}$ correlation state appears at 20.2 eV and a $^2B_{2u}$ correlation state appears at 22.2 eV. There is also a $^2A_g$ state at 22.1 eV and a $^2B_{3g}$ state at 21.9 eV but these states have very small pole strengths (see Table III).

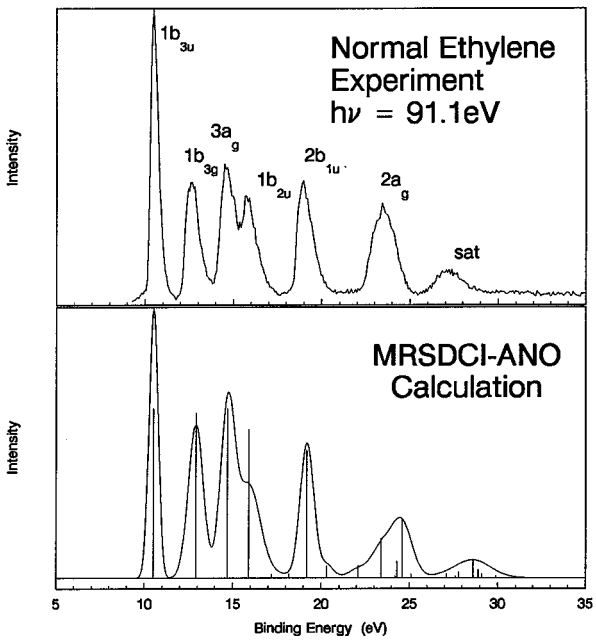


FIG. 13. Comparison of the normal ethylene spectrum taken at 91.1 eV (Fig. 1) with the final theoretical (MRSDCI-ANO) calculation [Table III and Fig. 12(c)]. It can be seen that the agreement is good in the inner valence region.

For the $^2B_{1g}$ and $^2A_u$ symmetries, only $1p$-$2h$ CI calculations were performed using canonical MOs. Because the first roots of the $^2B_{1g}$ and $^2A_u$ symmetries lie far above 30 eV binding energy with pole strengths on the order of $10^{-5}$ (see Table III), the possibility that the new correlation peak at 21.4 eV belongs to one of these two symmetries is excluded.

Overall, the final theoretical MRSDCI(ANO) PES fits the experimental spectra quite well especially in the inner valence region (see Fig. 13). Caution should be exercised in comparing the experimental *outer* valence region PES in Fig. 13 with the present theoretical calculations since the calculations do not include the dipole matrix elements and the peak intensities are simply proportional to $S_j^2$. The present theoretical results also clearly illustrates the subtleties and caveats of predicting the intensities and binding energies of correlation states even for a simple molecule like ethylene. The problems with assigning the symmetry of the correlation states at 27.4 and 21.4 eV is one point. Another is the twinning phenomenon which appears to be a real phenomenon and not a calculation artifact.

It is appropriate to point out that the twinning of the primary $^2A_g$ peak at 23.7 eV is not affected by using ISCI in the intensity (pole strength) calculation. From Table III, the

square of the coefficient of the leading hole state for each peak can be calculated. It is 0.21 ($0.46^2$) for the 23.4 eV line and 0.30 ($0.55^2$) for the 24.6 eV line. Then the ratio between these two lines is about 0.70, while the value calculated from the pole strengths which include ISCI is about 0.68.

Despite the general consistency, there is some disagreement between Tables III and IV in Murray and Davidson.[30] The peaks at 22.1 ($^2A_g$) and 29.6 eV ($^2B_{3g}$) were not found in the previous study.[30] The dual peaks at 23.4 and 24.6 eV of $^2A_g$ symmetry correspond to the previously reported[30] single peak at 23.7 eV and the intensities also have some disagreement. Comparing the present results with other studies, it is found that the twinning of the primary $^2A_g$ peak which was observed in the calculations of Cederbaum *et al.*[37] and Baker[38] is a true phenomenon, although the present calculation's intensity ratio is different. According to the MRS-DCI(ANO) calculation, the observable intensity in the 27.0–30.0 eV binding energy ''satellite region'' is a result of $^2A_g$ correlations only. All of the previous calculations[30,39–42] showed some intensity in this region from other symmetries. The present calculation gave many states of other symmetry in this energy region but none of these states had appreciable intensity.

### D. Origin of resonance structures

In this section we provide plausible explanations for the unexpected features found in the photon energy dependence of the cross sections of the new correlation peak (21.4 eV). As discussed in a previous letter,[28] the overall feature of increasing cross section towards threshold is indicative of dynamic correlations In particular, this feature is associated with continuum state configuration interaction otherwise known as conjugate shakeup.[66]

Following the phenomenology of Becker and Shirley,[3] the term ''shakeup'' is limited to correlation peaks that exhibit an increasing cross section with increasing photon energy (or kinetic energy) eventually reaching a plateau as the sudden limit is approached and therefore classified as dynamic correlation. However, historically the term shakeup took a broader definition[11,52] and refers to a photoionization process whereby an electron makes a dipole transition from orbital $i$ to continuum state $f$ accompanied by a ''monopole'' transition from orbital $m$ to orbital $n$. The shake-up transition moment is given by

$$M_{\text{shakeup}}=\langle f|\mu|i\rangle C_{(i^{-1}f)(i^{-1}m^{-1}nf)}, \tag{21}$$

where $C_{\alpha\beta}$ are the CI coefficients describing the ion in state $\beta$. This picture is akin to a common view that correlation states (shakeup) are due to ''ionization plus excitation processes.'' Clearly this mechanism may be considered as FISCI and thus can be classified as an intrinsic correlation; however we defer to the Becker–Shirley phenomenology—the framework which is the subject of the present investigation.

On the other hand, conjugate shakeup refers to a process whereby an electron makes a ''monopole'' transition from orbital $i$ to continuum state $f$ accompanied by a dipole transition from orbital $m$ to orbital $n$. The conjugate shake-up transition moment is given by

$$M_{\text{conjugate shakeup}}=\langle n|\mu|m\rangle C_{(m^{-1}n)(i^{-1}m^{-1}nf)}. \tag{22}$$

The relevant coefficients for calculation of relative photoionization cross sections are therefore $C_{(i^{-1}f)(i^{-1}m^{-1}nf)} \approx \langle n|m\rangle$ and $C_{(m^{-1}n)(i^{-1}m^{-1}nf)}\approx\langle f|i\rangle$ for shakeup and conjugate shakeup, respectively. The approximate relations of the CI coefficients to monopole matrix elements hold whenever separate sets of SCF optimized MOs are employed in the ion and the neutral as, e.g., in the relaxed Hartree–Fock approximation.[11] It can be shown[2] that the peak intensity of the conjugate process decreases like $\sim k^{-2}$ at large $k$. Here the continuum state is approximated by a plane wave with wave vector $k$.

Because of the high symmetry of ethylene and the specific excitations involved in the four candidate correlation states that might contribute to the 21.4 eV correlation peak, the shake-up process [Eq. (21)] cannot contribute significantly. *The conjugate shake-up process [Eq. (22)] is possible for all four candidate correlation states* ($^2A_g$, $^2B_{3g}$, $^2B_{1u}$, $^2B_{2u}$). The $^2A_g$ state with an outgoing electron of symmetry $b_{3u}$ can mix with, and get intensity from, the $na_g\leftarrow 1b_{3u}$ Rydberg excitation of neutral ethylene. The $^2B_{3g}$ state with an outgoing electron of symmetry $b_{2u}$, the $^2B_{1u}$ state with an outgoing electron of symmetry $a_g$, and the $^2B_{2u}$ state with an outgoing electron of symmetry $b_{3g}$ can all couple with the strong $\pi^*\leftarrow\pi$ excitation ($b_{2g}\leftarrow b_{3u}$) of neutral ethylene. Further, these last three states can also mix with each other through interchannel coupling since they all have overall symmetry $^1B_{1u}$. The leading configurations in these $N$-electron states (including the outgoing electron) differ from each other by double excitations so they can be strongly mixed by electron correlation effects.

Dynamic correlations such as conjugate shakeup have been observed in various atomic and molecular systems. Careful inspection of the photon energy dependence of the correlation states of helium,[15,67,68] lithium,[9] neon,[10] and CO[69] shows that the satellite intensity increases smoothly *to within 10 eV of threshold*. Very close to threshold (0–10 eV photoelectron kinetic energy) additional structure is generally observed and have been attributed to autoionization and/or shape resonance.

Autoionization, otherwise known as interchannel coupling,[3] refers to the decay of doubly excited states to different satellite channels (i.e., different excited states of the ion). These doubly excited states exert a significant influence on the correlation state cross sections. Interchannel coupling in atomic systems has been clearly illustrated in near threshold PES experiments of Wills *et al.*[70] as well as fluorescence measurements by Samson *et al.*[71] The resonance structures observed in these cases are strong and sharp (~200 meV FWHM) and occur within 10 eV of threshold. The resonance structures observed in the present experiment occur greater than 20 eV above threshold and are fairly broad structures (~8 eV FWHM). Since one cannot generalize interchannel coupling effects from the atomic case to a molecular case, we have searched for possible clues to doubly excited states. A survey of available photoionization and photoabsorption data on ethylene do not reveal anything extraordinary in the vicinity of the resonance photon energies (i.e., 42, 57, and

105 eV). The total photoabsorption data of Lee *et al.*[72] shows a smooth trend over 180–650 Å (69–19 eV). The inner valence photoionization cross section data of Brennan *et al.*[73] for the $2a_g^{-1}$ and $2b_{1u}^{-1}$ primary channels also do not show any clear structures in the 25–100 eV photon energy range. Likewise, the partial photoionization cross section data of Grimm *et al.*[74] for the $1b_{2u}^{-1}$ channel do not reveal any structure in the 12–26 eV photon energy range. Thus of the experimental data presently available, there is no strong evidence to suggest interchannel coupling.

Shape resonances[75] have been used to rationalize broad structures in the cross sections for photoionization and electron scattering of atoms and molecules. In a simplified sense for photoionization, the outgoing photoelectron experiences a superposition of polarization, exchange correlation, and centrifugal potentials which provides a barrier into the inner region of the potential energy curve. This barrier, otherwise known as the anisotropic molecular field, allows for the ''trapping'' of the photoelectron at particular energies known as the shape resonance energies. Shape resonance has been invoked as a rationalization for broad structures observed in the photon energy dependence of the core correlation state cross sections of $N_2$[76] and CO.[69] In the case of CO, a shape resonance in the *K*-shell $\pi \rightarrow \pi^*$ correlation states was predicted in theoretical calculations by McCoy *et al.*[77] and Lucchese *et al.*[78] This shape resonance was recently observed by Reich *et al.*[69] although at slightly lower photon energy. The photon energy dependence curve shows the width (~5 eV FWHM) of the single shape resonance in a *K*-shell correlation state of CO[69] to be consistent with the widths observed in ethylene (~8 eV FWHM). The only difference is that in the photon energy dependence curve of the inner valence correlation state of ethylene more than one broad structure is observed. Thus it is difficult to explain the multiresonance structure within the framework of simple shape resonance theory.[75] A recent multichannel configuration interaction method[78] appears to be promising for the present case. Many-channel effects have been shown to be more critical in describing the satellite states as compared to the primary ion states.

Another possible interpretation was also advanced in an earlier report.[28] The multiresonance features can be considered as oscillations superimposed on a smoothly increasing cross section towards threshold. Thus we attempt to characterize these oscillations in Sec. IV B. We find that the Fourier transform of the purely oscillating fraction of the correlation state cross section yields two characteristic distances, namely 0.6 and 2.2 Å. It is interesting to note that these distances are simple fractions ($R_0/2$ and $3R_0/2$) of the C–C bond length in ethylene ($R_0$=1.34 Å). Further theoretical and experimental into these observations would be most useful.

The MRSDCI(ANO) calculations indicate that the new correlation peak at 21.4 eV can be either a $^2B_{1u}$ state predicted at 20.2 eV, a $^2B_{2u}$ state predicted at 22.2 eV, a $^2A_g$ state at 22.1 eV, or a $^2B_{3g}$ state at 21.9 eV. The $^2B_{1u}$ state is predominantly a $3a_g^{-1}(\pi \rightarrow \pi^*)$ process with intensity borrowed from the $2b_{1u}^{-1}$ primary hole whereas the $^2B_{2u}$ state is predominantly a $1b_{3g}^{-1}(\pi \rightarrow \pi^*)$ process with intensity borrowed from the $1b_{2u}^{-1}$ primary hole. The calculated pole strengths for the $^2B_{1u}$ and $^2B_{2u}$ states are the same (0.06). Note that the present MRSDCI(ANO) calculations apply only to the intrinsic component and do not include some dynamic components (e.g., conjugate shakeup) since bound–free mixing between highly excited neutrals and free electron neutrals are not included. On this point we can also consider the $^2A_g$ and $^2B_{3g}$, both with zero pole strengths, as likely candidates; but without detailed calculations (e.g., bound–free mixing) anything further is premature.

Whereas arguments based on general observations regarding the tendency of MRSDCI calculations to overestimate energy separations would support a $^2B_{2u}$ assignment, estimates of the experimental $\beta$ parameter for the new correlation peak would support a $^2B_{1u}$ symmetry assignment. Still there is no strong evidence to decide between any of the four candidate correlation states. A clue lies perhaps in a simple analysis of some of the candidate correlation states. Consider the occupied valence orbitals and lowest unoccupied orbital (Kimura notation) of ethylene:

$$2a_g(\sigma)2b_{1u}(\sigma^*)1b_{2u}(\pi^+_{CH2})3a_g(\sigma_{CC}) \times 1b_{3g}(\pi^-_{CH2})1b_{3u}(\pi)1b_{2g}(\pi^*).$$

Relative to the primary hole ($\sigma^* \rightarrow$ *continuum*), the $^2B_{1u}$ satellite arises from a ($\sigma^* \leftarrow \sigma_{CC}, \pi \rightarrow \pi^*$) double excitation wherein a *particle* excited to a $\pi^*$ orbital is offset by a *hole* ($\sigma^*$) excited to $\sigma_{CC}$. As discussed by Martin and Davidson,[36] this ''one-down one-up'' process takes very little energy and plays an important role in very intense satellites. Relative to the primary hole ($\pi^+_{CH2} \rightarrow$ *continuum*), the $^2B_{2u}$ satellite arises from a ($\pi^+_{CH2} \leftarrow \pi^-_{CH2}, \pi \rightarrow \pi^*$) double excitation wherein the *particle* excited to a $\pi^*$ orbital is offset by a *hole* ($\pi^+_{CH2}$) excited to $\pi^-_{CH2}$.

In summary, synchrotron PES experiments indicate that the new correlation peak at 21.4 eV is a dynamic correlation and most likely associated with a conjugate shake-up process. MRSDCI(ANO) calculations indicate four possible correlation states ($^2B_{1u}, ^2B_{2u}, ^2A_g, ^2B_{3g}$) corresponding to this new correlation peak. The exact origin of the observed oscillations in the new correlation peak/$2b_{1u}$ intensity ratio as a function of photon energy is still unknown.

## ACKNOWLEDGMENTS

We would like to acknowledge the assistance of the staff of the Synchrotron Radiation Center, University of Wisconsin. We would also like to thank H. Sadeghpour, C. D. Lin, J. L. Dehmer, and J. A. R. Samson for helpful discussions. This work was funded by the Natural Sciences and Engineering Research Council of Canada. The work at Indiana University was supported by the National Science Foundation.

[1] R. L. Martin and D. A. Shirley, J. Chem. Phys. **64**, 3685 (1976); Phys. Rev. A **13**, 1475 (1976).
[2] L. S. Cederbaum, W. Domcke, J. Schirmer, and W. von Niessen, Adv. Chem. Phys. **65**, 115 (1986).
[3] U. Becker and D. A. Shirley, Phys. Scr. **T31**, 56 (1990).
[4] F. Wuilleumier and M. O. Krause, Phys. Rev. A **10**, 242 (1974).
[5] T. D. Thomas, Phys. Rev. Lett. **52**, 417 (1984).
[6] U. Becker, R. Hölzel, H. G. Kerkhoff, B. Langer, D. Szostak, and R. Wehlitz, Phys. Rev. Lett. **56**, 1120 (1986).
[7] P. A. Heimann, U. Becker, H. G. Kerkhoff, B. Langer, D. Szostak, R.

Wehlitz, D. W. Lindle, T. A. Ferrett, and D. A. Shirley, Phys. Rev. A **34**, 3782 (1986).
[8] A. D. O. Bawagan, B. J. Olsson, K. H. Tan, J. M. Chen, and G. M. Bancroft, Chem. Phys. Lett. **179**, 344 (1991).
[9] T. A. Ferrett, D. W. Lindle, P. A. Heimann, W. D. Brewer, U. Becker, H. G. Kerkhoff, and D. A. Shirley, Phys. Rev. A **36**, 3172 (1987).
[10] U. Becker (1989), quoted on p. 1591 in V. Schmidt, Rep. Progr. Phys. **55**, 1483 (1992).
[11] K. G. Dyall and F. P. Larkins, J. Phys. B **15**, 203, 219 (1982); J. A. Richards and F. P. Larkins, J. Electron. Spectrosc. Relat. Phenom. **32**, 193 (1983).
[12] U. Gelius, J. Electron. Spectrosc. Relat. Phenom. **5**, 985 (1974).
[13] M. A. Brisk and A. D. Baker, J. Electron. Spectrosc. Relat. Phenom. **7**, 197 (1975).
[14] M. Y. Adam, F. Wuilleumier, S. Krummacher, N. Sander, V. Schmidt, and W. Mehlhorn, J. Electron. Spectrosc. Relat. Phenom. **15**, 211 (1979).
[15] D. W. Lindle, T. A. Ferrett, U. Becker, P. H. Kobrin, C. M. Truesdale, H. G. Kerkhoff, and D. A. Shirley, Phys. Rev. A **31**, 714 (1985).
[16] D. W. Lindle, P. A. Heimann, T. A. Ferrett, P. H. Kobrin, C. M. Truesdale, U. Becker, H. G. Kerkhoff, and D. A. Shirley, Phys. Rev. A **33**, 319 (1986).
[17] U. Becker, H. G. Kerkhoff, D. W. Lindle, P. H. Kobrin, T. A. Ferrett, P. A. Heimann, C. M. Truesdale, and D. A. Shirley, Phys. Rev. A **34**, 2858 (1986).
[18] C. E. Brion, A. O. Bawagan, and K. H. Tan, Chem. Phys. Lett. **134**, 76 (1987).
[19] H. Kossmann, B. Krässig, V. Schmidt, and J. E. Hansen, Phys. Rev. Lett. **58**, 1620 (1987).
[20] U. Becker, B. Langer, H. G. Kerkhoff, M. Kupsch, D. Szostak, R. Wehlitz, P. A. Heimann, S. H. Liu, D. W. Lindle, T. A. Ferrett, and D. A. Shirley, Phys. Rev. Lett. **60**, 1490 (1988).
[21] C. E. Brion, A. O. Bawagan, and K. H. Tan, Can. J. Chem. **66**, 1877 (1988).
[22] J. Tulkki, Phys. Rev. Lett. **62**, 2817 (1989).
[23] T. A. Ferrett, D. W. Lindle, P. A. Heimann, H. G. Kerkhoff, U. E. Becker, and D. A. Shirley, Phys. Rev. A **34**, 1916 (1986).
[24] A. Reimer, J. Schirmer, J. Feldhaus, A. M. Bradshaw, U. Becker, H. G. Kerkhoff, B. Langer, D. Szostak, and R. Wehlitz, Phys. Rev. Lett. **57**, 1707 (1986).
[25] A. D. O. Bawagan, B. J. Olsson, K. H. Tan, J. M. Chen, and B. X. Yang, Chem. Phys. **164**, 283 (1992).
[26] B. Sjörgen, S. Svensson, A. Naves de Brito, N. Correia, M. P. Keane, and C. Enkvist, J. Chem. Phys. **96**, 6389 (1992).
[27] S. J. Desjardins, A. D. O. Bawagan, and K. H. Tan, Chem. Phys. Lett. **196**, 261 (1992).
[28] S. J. Desjardins, A. D. O. Bawagan, K. H. Tan, Y. Wang, and E. R. Davidson, Chem. Phys. Lett. **227**, 519 (1994).
[29] C. D. Lin, Phys. Rev. A **9**, 171 (1974).
[30] C. W. Murray and E. R. Davidson, Chem. Phys. Lett. **190**, 231 (1992).
[31] A. Berndtsson, E. Basilier, U. Gelius, J. Hedman, M. Klasson, R. Nilsson, C. Nordling, and S. Svensson, Phys. Scr. **12**, 235 (1975).
[32] M. S. Banna and D. A. Shirley, J. Electron. Spectrosc. Relat. Phenom. **8**, 255 (1976).
[33] G. Bieri and L. Åsbrink, J. Electron. Spectrosc. Relat. Phenom. **20**, 149 (1980).
[34] M. P. Keane, A. Naves de Brito, N. Correia, S. Svensson, L. Karlsson, B. Wannberg, U. Gelius, S. Lunell, W. R. Salaneck, M. Lögdlund, D. B. Swanson, and A. G. MacDiarmid, Phys. Rev. B **45**, 6390 (1992).
[35] W. von Niessen, G. H. F. Diercksen, L. S. Cederbaum, and W. Domcke, Chem. Phys. **18**, 469 (1976).
[36] R. L. Martin and E. R. Davidson, Chem. Phys. Lett. **51**, 237 (1977).
[37] L. S. Cederbaum, W. Domke, J. Schirmer, W. von Niessen, G. H. F. Diercksen, and W. P. Kraemer, J. Chem. Phys. **69**, 1591 (1978).
[38] J. Baker, Chem. Phys. Lett. **101**, 136 (1983).
[39] H. Nakatsuji, J. Chem. Phys. **80**, 3703 (1984).
[40] H. Wasada and K. Hirao, Chem. Phys. **138**, 277 (1989).
[41] E. Lindholm and L. Åsbrink, J. Electron. Spectrosc. Relat. Phenom. **18**, 121 (1980).
[42] M. A. Coplan, A. L. Migdall, J. H. Moore, and J. A. Tossell, J. Am. Chem. Soc. **100**, 5008 (1978).
[43] A. J. Dixon, S. T. Hood, E. Weigold, and G. R. J. Williams, J. Electron. Spectrosc. Relat. Phenom. **14**, 267 (1978).
[44] I. E. McCarthy, J. Electron. Spectrosc. Relat. Phenom. **36**, 37 (1985).
[45] A. S. Kheifets and M. Ya. Amusia, Phys. Rev. A **46**, 1261 (1992).
[46] S. Braidwood, M. Brunger, and E. Weigold, Phys. Rev. A **47**, 2927 (1993).
[47] A. D. O. Bawagan, J. Phys. (Paris) **C6**, 175 (1993).
[48] Z. F. Liu, G. M. Bancroft, L. L. Coatsworth, and K. H. Tan, Chem. Phys. Lett. **203**, 337 (1993).
[49] K. H. Tan, G. M. Bancroft, L. L. Coatsworth, and B. W. Yates, Can. J. Phys. **60**, 131 (1982).
[50] B. P. Tonner and E. W. Plummer, Nucl. Instrum. Methods **177**, 153 (1980).
[51] J. D. Bozek, J. N. Cutler, G. M. Bancroft, L. L. Coatsworth, K. H. Tan, D. S. Yang, and R. G. Cavell, Chem. Phys. Lett. **165**, 1 (1990).
[52] T. Åberg, Phys. Rev. **156**, 35 (1967).
[53] R. L. Martin, B. E. Mills, and D. A. Shirley, J. Chem. Phys. **64**, 3690 (1976).
[54] G. Bieri, F. Burger, E. Heilbronner, and J. P. Maier, Helv. Chim. Acta **60**, 2213 (1977).
[55] P. G. Wilkinson and R. S. Mulliken, J. Chem. Phys. **23**, 1895 (1955).
[56] J. E. Pollard, D. J. Trevor, J. E. Reutt, Y. T. Lee, and D. A. Shirley, J. Chem. Phys. **81**, 5302 (1984).
[57] H. Koppel, W. Domcke, L. S. Cederbaum, and W. von Niessen, J. Chem. Phys. **69**, 4252 (1978).
[58] L. S. Cederbaum and F. Tarantelli, J. Chem. Phys. **98**, 9691 (1993).
[59] J. Muller, R. Arneberg, H. Agren, R. Manne, P. A. Malmquist, S. Svensson, and U. Gelius, J. Chem. Phys. **77**, 4895 (1982).
[60] H. Partridge, in NASA Technical Memorandum 101044 (1989), p. 73.
[61] H. Partridge, in NASA Technical Memorandum 89449 (1987), p. 73.
[62] C. J. Maxwell, F. B. C. Machado, and E. R. Davidson, J. Am. Chem. Soc. **114**, 6496 (1992).
[63] T. H. Dunning, Jr., J. Chem. Phys. **90**, 1007 (1989).
[64] Y. Wang, Ph.D. thesis, Indiana University (1994); D. Feller and E. R. Davidson, J. Chem. Phys. **74**, 3977 (1981).
[65] D. F. Evans, J. Chem. Soc. **2**, 1735 (1960).
[66] T. Ishihara, J. Mizuno, and T. Watanabe, Phys. Rev. A **22**, 1552 (1980).
[67] J. A. R. Samson, Phys. Rev. Lett. **22**, 693 (1969).
[68] F. Wuilleumier, M. Y. Adam, N. Sandner, and V. Schmidt, J. Phys. (Paris) Lett. **41**, 373 (1980).
[69] T. Reich, P. A. Heimann, B. L. Petersen, E. Hudson, Z. Hussain, and D. A. Shirley, Phys. Rev. A **49**, 4570 (1994).
[70] A. A. Wills, A. A. Cafolla, A. Svensson, and J. Comer, J. Phys. B **23**, 2013 (1990).
[71] J. A. R. Samson, Y. Chung, and E. M. Lee, Phys. Rev. A **45** 259 (1992).
[72] L. C. Lee, R. W. Carlson, D. L. Judge, and M. Ogawa, J. Quant. Spectrosc. Radiat. Transfer **13**, 1023 (1973).
[73] J. G. Brennan, G. Cooper, J. C. Green, M. P. Payne, and C. MN. Redfern, J. Electron. Spectrosc. Relat. Phenom. **43**, 297 (1987).
[74] F. A. Grimm, T. A. Whitley, P. R. Keller, and J. W. Taylor, Chem. Phys. **154**, 303 (1991).
[75] J. L. Dehmer and D. Dill, in *Electron–Molecule and Photon–Molecule Collisions*, edited by T. Rescigno, V. McKoy, and B. Schneider (Plenum, New York, 1979), pp. 225–265.
[76] S. Krummacher, V. Schmidt, and F. Wuilleumier, J. Phys. B **13**, 3993 (1980).
[77] J. Schirmer, M. Braunstein, and V. McCoy, Phys. Rev. A **44**, 5762 (1991).
[78] G. Bandarage and R. R. Lucchese, Phys. Rev. A **47**, 1989 (1993).